Fields and fracture of the interface between a glassy polymer and a rigid substrate

Wang, GF; Van der Giessen, E

Published in:
European Journal of Mechanics A-Solids

DOI:
10.1016/j.euromechsol.2004.03.001

Available online at www.sciencedirect.com
SCIENCE DIRECT®
European Journal of Mechanics A/Solids 23 (2004) 395–409

Fields and fracture of the interface between a glassy polymer and a rigid substrate

G.F. Wang, E. Van der Giessen *

University of Groningen, Department of Applied Physics, Nijenborgh 4, 9747 AG, Groningen, The Netherlands

Received 27 October 2003; accepted 3 March 2004

Available online 10 April 2004

Abstract

In this paper, the plane-strain finite deformations near the tip of a blunted crack between a viscoplastic glassy polymer and a rigid substrate are investigated assuming small-scale yielding. A constitutive model accounting for the intrinsic softening upon yield and the subsequent orientational strain hardening is adopted to simulate the typical behavior of glassy polymers. The influence of mode mixity and plasticity characteristics on the near-tip fields is studied. The distribution of interface normal stress, as the cause of interface delamination, is analyzed. Based on these results, a simple delamination criterion involving an interface bond strength is adopted to estimate the interface toughness. The interface bond strength governs the extent of plastic deformation that can accumulate prior to interface delamination, and the contribution of plastic dissipation to the interface toughness depends on the mode mixity and the plasticity characteristics.

Keywords: Polymer; Interface; Fracture; Plasticity; Toughness; Mode mixity

1. Introduction

Proper adhesion is critical for many engineering materials, such as composites. A particular class of multi-component materials is that involving polymers and metals. Sandwich materials are among the most known ones, such as Hylite®[1] with a thermoplastic polymer sheet between two very thin aluminum sheets. Although being exciting candidates for lightweight applications, this kind of material is often limited by the adhesion between the polymer and the metal. Experimental characterization of adhesion is complicated by the fact that adhesion is a property of the material system and not of the interface alone. In particular, adhesion as characterized by the fracture toughness in a chosen experiment, is strongly dependent on the deformation properties of the two binded materials (see, e.g., Cao and Evans, 1989; Wang and Suo, 1990). For bi-material systems where at least one of the materials is ductile, the plastic work dissipated in the fracture process may contribute a large part to the total work.

Much is known about the mechanics involved in metal-ceramic systems (e.g., Hutchinson and Evans, 2000; Wei and Hutchinson, 1999) but less for systems involving polymers. Extrapolation of the results for plasticity in a metal to that in a polymer can be misleading since the plasticity in a polymer has significantly different characteristics (intrinsic softening after yield followed by progressive re-hardening; Bowden, 1973) than that in a metal. One consequence of this is that the plastic zone near the crack tip in a polymer is distinctly different from that in a metal (Lai and Van der Giessen, 1997; Basu and Van der Giessen, 2002). Thus, although a complete analysis of interfacial debonding also requires a description

* Corresponding author.
E-mail address: giessen@phys.rug.nl (E. Van der Giessen).
[1] Registered Trademark of Corus Hylite BV.

0997-7538/$ – see front matter
doi:10.1016/j.euromechsol.2004.03.001

of the interface, in terms of, for instance, a cohesive law (Needleman, 1990; Tvergaard and Hutchinson, 1993), we consider it useful to first study the near-tip fields for a crack along a polymer–metal interface. As the elastic modulus and the yield strength of the metals involved are significantly larger than those of the polymers used, the metal can be treated as being rigid.

The paper is organized in the following way. The constitutive relationship of the glassy amorphous polymer is briefly reviewed in Section 2. Then the mathematical model and the solution method are presented in Section 3. In Section 4, the effects of mode mixity and the softening–hardening characteristics on the plastic deformation near an interfacial crack tip are investigated. Finally, a simple delamination criterion is adopted to assess the contribution of plasticity to the interface toughness.

2. Constitutive model of glassy polymer

For the glassy amorphous polymer, we adopt the elastic–viscoplastic model proposed by Boyce et al. (1988) and later modified by Wu and Van der Giessen (1993). This model incorporates the initial elastic response and the rate-dependent yielding of polymers, including the intrinsic softening upon yield and the nonlinear strain hardening at large plastic deformations. Referring to Wu and Van der Giessen (1993) for details, the model is summarized as follows.

The Eulerian strain rate $\mathbf{D}$ is decomposed into an elastic part $\mathbf{D}^{\mathrm{e}}$ and a plastic part $\mathbf{D}^{\mathrm{p}}$

$$\mathbf{D} = \mathbf{D}^{\mathrm{e}} + \mathbf{D}^{\mathrm{p}}. \tag{1}$$

Assuming the elastic strain to be small, the elastic strain rate $\mathbf{D}^{\mathrm{e}}$ is expressed by the hyper-elastic law

$$\mathbf{D}^{\mathrm{e}} = \mathfrak{R}^{-1}\overset{\nabla}{\boldsymbol{\sigma}}, \tag{2}$$

in terms of the Jaumann derivative of the Cauchy stress tensor $\boldsymbol{\sigma}$, $\overset{\nabla}{\boldsymbol{\sigma}} = \dot{\boldsymbol{\sigma}} - \mathbf{W}\boldsymbol{\sigma} + \boldsymbol{\sigma}\mathbf{W}$, where $\mathbf{W}$ is the continuum spin tensor. $\mathfrak{R}$ is the standard fourth-order tensor of isotropic elastic moduli with Cartesian components

$$\mathfrak{R}_{ijkl} = \frac{E}{2(1+\nu)}\left(\delta_{ik}\delta_{jl} + \delta_{il}\delta_{jk} + \frac{2\nu}{1-2\nu}\delta_{ij}\delta_{kl}\right), \tag{3}$$

where E is Young's modulus and ν is Poisson's ratio.

According to Argon's (1973) model of yield in glassy polymers, the equivalent plastic shear strain rate $\dot{\gamma}^{\mathrm{p}}$ caused by an applied shear stress τ is given by

$$\dot{\gamma}^{\mathrm{p}} = \dot{\gamma}_0 \exp\left\{-\frac{As_0}{T}\left[1 - \left(\frac{\tau}{s_0}\right)^{5/6}\right]\right\}, \tag{4}$$

where $\dot{\gamma}_0$ and A are material parameters, T is the absolute temperature, and s_0 is the athermal shear strength. To incorporate the effect of pressure $p = -\operatorname{tr}\boldsymbol{\sigma}/3$ on plastic flow and the effect of strain softening, s_0 is replaced by $s + \alpha p$ with α the pressure sensitivity parameter. The current shear strength s is assumed to evolve from the initial value s_0 with plastic straining by

$$\dot{s} = h\left(1 - \frac{s}{s_{\mathrm{ss}}}\right)\dot{\gamma}^{\mathrm{p}}, \tag{5}$$

where h is a material parameter and s_{ss} is the saturation value of s. The plastic strain rate tensor is determined by

$$\mathbf{D}^{\mathrm{p}} = \dot{\gamma}^{\mathrm{p}}\frac{\bar{\boldsymbol{\sigma}}'}{\sqrt{2}\,\tau}, \quad \tau = \sqrt{\frac{1}{2}\bar{\boldsymbol{\sigma}}' : \bar{\boldsymbol{\sigma}}'}, \tag{6}$$

where $\bar{\boldsymbol{\sigma}}'$ is the deviatoric part of the driving stress $\bar{\boldsymbol{\sigma}}$. The driving force for plastic flow is

$$\bar{\boldsymbol{\sigma}} = \boldsymbol{\sigma} - \mathbf{b}, \tag{7}$$

where $\mathbf{b}$ is the back stress tensor accounting for the orientational strain hardening of the material. In terms of the corresponding principal plastic stretches λ_α, the back stress $\mathbf{b}$ can be expressed as follows:

$$\mathbf{b} = \sum_\alpha b_\alpha\left(\mathbf{e}_\alpha^{\mathrm{p}} \otimes \mathbf{e}_\alpha^{\mathrm{p}}\right), \quad b_\alpha = b_\alpha(\lambda_\beta), \tag{8}$$

where b_α are the principal components of $\mathbf{b}$ on the unit principal directions $\mathbf{e}_\alpha^{\mathrm{p}}$ of the left plastic stretch tensor. According to the numerical calculations of Wu and Van der Giessen (1993), the back stress can be captured accurately by the following combination of the classical three-chain network description and the recent Arruda and Boyce (1993) eight-chain model:

$$b_\alpha = (1-\rho)b_\alpha^{\text{3-ch}} + \rho b_\alpha^{\text{8-ch}}, \tag{9}$$

where the weight factor ρ is determined by the maximum plastic stretch $\bar{\lambda} = \max(\lambda_1, \lambda_2, \lambda_3)$ through $\rho = 0.85\bar{\lambda}/\sqrt{N}$. Here N is a polymer-chain parameter, which determines the limit stretch $\lambda_{\max}$ of a molecular chain as $\lambda_{\max} = \sqrt{N}$. Furthermore in Eq. (9)

$$b_\alpha^{3\text{-ch}} = \frac{1}{3} C^{\mathrm{R}} \sqrt{N} \lambda_\alpha \mathcal{L}^{-1}\left(\frac{\lambda_\alpha}{\sqrt{N}}\right), \tag{10}$$

$$b_\alpha^{8\text{-ch}} = \frac{1}{3} C^{\mathrm{R}} \sqrt{N} \frac{\lambda_\alpha^2}{\lambda_{\mathrm{c}}} \mathcal{L}^{-1}\left(\frac{\lambda_{\mathrm{c}}}{\sqrt{N}}\right), \quad \lambda_{\mathrm{c}} = \frac{1}{3}\sum_{\alpha=1}^{3} \lambda_\alpha^2, \tag{11}$$

where C^{R} is a material constant and $\mathcal{L}^{-1}$ is the inverse of the Langevin function $\mathcal{L}(\beta) = \coth(\beta) - 1/\beta$.

For the convenience of later use, we note that the dissipated plastic work in a body of volume V can be expressed as

$$W_{\mathrm{p}} = \int_0^t \int_V \bar{\boldsymbol{\sigma}} : \mathbf{D}^{\mathrm{p}} \, \mathrm{d}V \, \mathrm{d}t = \int_0^t \int_V \sqrt{2}\tau \dot{\gamma}^{\mathrm{p}} \, \mathrm{d}V \, \mathrm{d}t. \tag{12}$$

Note that part of the plastic work rate $\boldsymbol{\sigma} : \mathbf{D}^{\mathrm{p}}$ is stored in the stretched molecular network; see Basu and Van der Giessen (2002) for more details.

It should be pointed out that in present model, when λ_α or λ_{c} approaches the chain limit stretch $\lambda_{\max}$, the hardening rate provided by the increased network stiffness accelerates enormously, and thereby suppresses all further plastic flow: the network 'locks'. Therefore, when either λ_α or λ_{c} exceeds $0.99\lambda_{\max}$, viscoplastic flow is disabled in the calculation ($\dot{\gamma}^{\mathrm{p}} = 0$), so that $\mathbf{D}^{\mathrm{p}} = 0$.

3. Model and method of solution

We perform a small-scale yielding analysis for a crack on the interface between a polymer and a rigid substrate, which represents a much stiffer metal. Plasticity in the polymer is assumed to be confined to a region around the tip that is much smaller than the radius of outer boundary R_∞. The crack is assumed to be blunt with a root-radius r_t. Not only is this more realistic than a mathematically sharp crack, it also avoids contact between crack surfaces. Because the rigid substrate gives no contribution to deformation but provides the constraint on the interface, only the upper-half of the region, corresponding to the polymer, is investigated as shown in Fig. 1(a). A Cartesian (x_1, x_2) coordinate system is set up with the origin at the crack tip and the x_1-axis along the interface.

The elastic solution governing the remote field in small-scale yielding of an interfacial crack is the dominant crack tip singularity field. This field predicts the tractions on the interface to be given by

$$\sigma_{22} + \mathrm{i}\sigma_{12} = \frac{K}{\sqrt{2\pi x_1}} r^{\mathrm{i}\varepsilon}, \tag{13}$$

with $r = \sqrt{x_1^2 + x_2^2}$ and

$$K = K_1 + \mathrm{i}K_2, \quad \mathrm{i} = \sqrt{-1}, \quad |K| = \sqrt{K_1^2 + K_2^2}, \tag{14}$$

where K_1 and K_2 are the mode I and mode II stress intensity factors, respectively. The oscillatory index ε is related to the second Dundurs parameter β by

$$\varepsilon = \frac{1}{2\pi} \ln\left(\frac{1-\beta}{1+\beta}\right), \tag{15}$$

which for an elastic–rigid material system is simply given by

$$\beta = -\frac{1}{2}\left(\frac{1-2\nu}{1-\nu}\right). \tag{16}$$

We use the measure of mode mixity defined by Rice (1988),

$$\psi = \arctan\left[\frac{\mathrm{Im}(KL^{\mathrm{i}\varepsilon})}{\mathrm{Re}(KL^{\mathrm{i}\varepsilon})}\right], \tag{17}$$

where $\mathrm{Re}(\cdot)$ and $\mathrm{Im}(\cdot)$ denote the real and imaginary parts of a complex quantity, respectively, and L is a reference length. From Eq. (13), one sees that ψ indicates the relative proportion of shear to normal stress on the interface at a distance L from

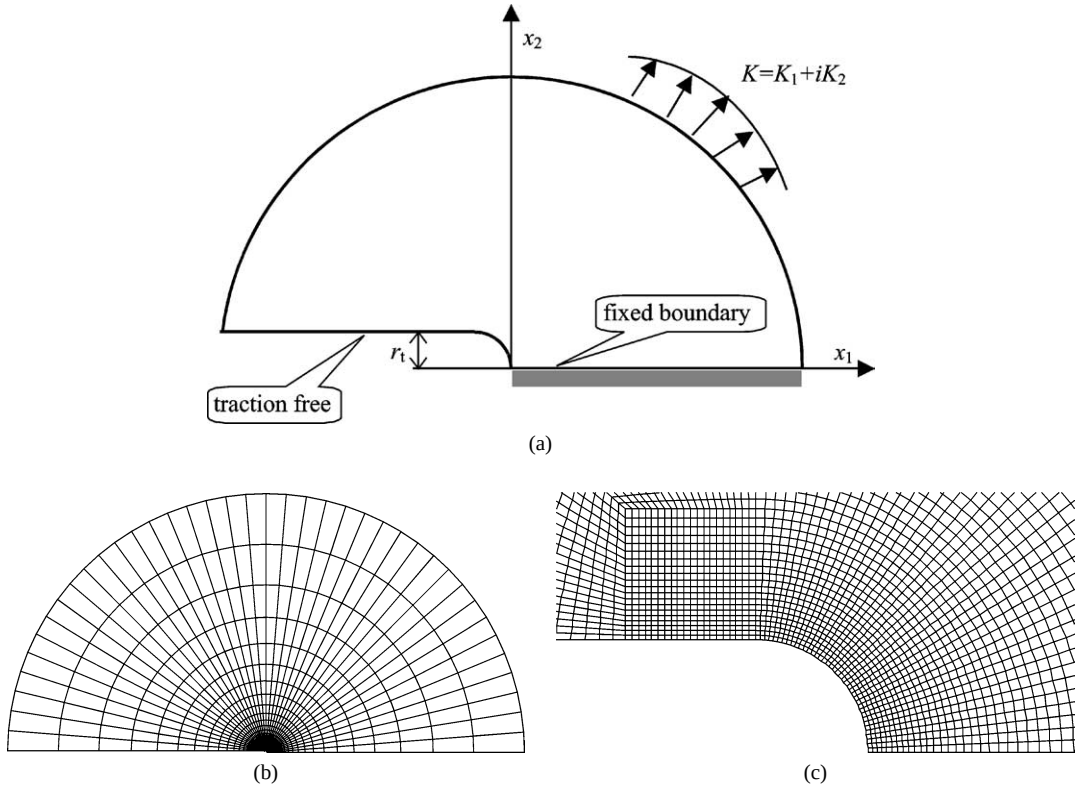

Fig. 1. (a) Schematic of the interfacial problem; (b) the finite element mesh (actual scale); (c) the near-tip mesh.

the crack tip. When $\varepsilon = 0$, ψ reduces to the familiar measure with $\tan\psi = K_2/K_1$. The definition of mode mixity is directly associated with L, and different values of L give rise to a shift of ψ. For a meaningful comparison of various loading cases, the same value of L must be used. A proper choice of L, such as the plastic zone size or the relevant microstructure length, is advantageous to interpret the mixed mode fracture data.

The energy release rate $\mathcal{G}$ is related to K by

$$\mathcal{G} = \left(1-\beta^2\right)\frac{1-\nu^2}{2E}|K|^2. \tag{18}$$

Within the small-scale yielding framework, remote loading is prescribed in terms of the elastic displacements along $r = R_\infty$, given by

$$u_1 + \mathrm{i}u_2 = \frac{2(1+\nu)}{E}\frac{|K|r^{1/2}}{2\sqrt{2\pi}\cosh(\pi\varepsilon)}\left[\frac{(3-4\nu)\exp(\bar{\theta}-\mathrm{i}\bar{\psi}) - \exp(-\bar{\theta}-\mathrm{i}\bar{\psi})}{1-2\mathrm{i}\varepsilon} - \mathrm{i}\sin\theta\exp(\bar{\theta}+\mathrm{i}\bar{\psi})\right] \tag{19}$$

with

$$\theta = \arctan\left(\frac{x_2}{x_1}\right), \quad \bar{\theta} = \frac{\mathrm{i}\theta}{2} + \varepsilon(\theta-\pi), \quad \bar{\psi} = \psi + \varepsilon\ln\left(\frac{r}{L}\right). \tag{20}$$

On the crack surface, traction-free conditions are assumed

$$\sigma_{12}(x_1,0) = \sigma_{22}(x_1,0) = 0 \quad \text{for } x_1 < 0, \tag{21}$$

while on the interface, the displacements are prescribed to be

$$u_1(x_1,0) = u_2(x_1,0) = 0 \quad \text{for } x_1 \geqslant 0, \tag{22}$$

owing to the constraint of the rigid substrate.

With these boundary conditions, a finite strain, quasi-static finite element analysis of the full-field, near-tip problem is carried out. The procedure follows the previous work of Lai and Van der Giessen (1997), based on a linear incremental form of the

virtual work principle, augmented with an equilibrium correction and an adaptive time stepping method; details can be found in (Wu and Van der Giessen, 1996). Quadrilateral elements are adopted, each of which is built up of four linear velocity, triangular subelements arranged in a 'crossed triangle' configuration. With a proper aspect ratio and orientation, these elements are well suited to pick up localized deformation. Fig. 1(b) and (c) show the finite element mesh used in the numerical calculation.

In our numerical calculation, the root-radius of the blunted crack tip r_t is taken as 0.1 mm; the radius of the remote boundary R_∞ is about $165r_t$, which is large enough to provide K dominance for the near-tip deformation. L is taken equal to 0.1 mm, as in the experimental procedure of Wang and Suo (1990).

4. Stress and deformation fields

To gain some understanding of interfacial fracture involving polymers, the calculations are carried out in the following order. Firstly, the influence of mode mixity on the near-tip plastic deformation is discussed in detail for a typical polymer, referred to as material A. Then material B, which exhibits no softening but progressive hardening after yield, and material C, which shows only softening but no re-hardening, are dealt with to investigate the effects of strain softening and hardening on the development of the plastic zone. Detailed material parameters are given in Table 1. Materials A, B and C in the present paper correspond to materials C, B and E respectively in Lai and Van der Giessen (1997), but with a smaller value of C^R. The uniaxial stress–strain behavior for each of these materials is plotted in Fig. 2 for reference.

Subsequently, the influence of plastic deformation on the interface normal stress is analyzed. Based on these results, the influence of plasticity and of mode mixity on interface toughness are discussed through an imposed delamination criterion involving normal stress.

4.1. Influence of mode mixity

We first study the interface between material A and a rigid substrate, by applying three loading modes: (a) $K_1 > 0$, $K_2 = 0$ ($\psi = -7.06°$); (b) $K_1 = 0$, $K_2 > 0$ ($\psi = 82.94°$); and (c) $K_1 = -K_2 > 0$ ($\psi = -52.06°$). Different combinations of K_1 and K_2 indicate the variation of the tensile to shear loading ratio.

Table 1
Material parameters

Material	ν	E/s_0	s_{ss}/s_0	As_0/T	α	h/s_0	N	C^R/s_0
A	0.4	9.38	0.79	79.2	0.08	5.15	2.8	0.07
B	0.4	9.38	1	79.1	0.08	0	2.8	0.07
C	0.4	9.38	0.79	79.2	0.08	5.15	100	0

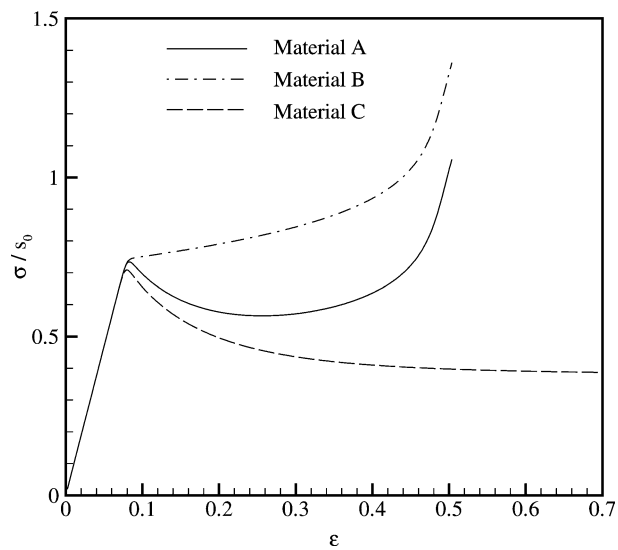

Fig. 2. Uniaxial stress–strain behavior for different materials.

To present the shape of the initial yield zone and the subsequent propagation of localized plastic shearing, contours of instantaneous plastic shear rate $\dot{\gamma}^{\mathrm{p}}$ are plotted. Note that rather than accumulated plastic strain, this shows the distribution of the current plastic flow *activity*. For convenience, the plastic strain rate is normalized by a strain rate quantity $\dot{\Gamma}$ defined by

$$\dot{\Gamma} = |\dot{K}|/K_0, \tag{23}$$

with $K_0 = s_0\sqrt{r_{\mathrm{t}}}$ and $|\dot{K}| = 35\ \mathrm{MPa}\sqrt{\mathrm{mm}}\,s^{-1}$ in our calculation. All coordinates are normalized by the initial root-radius of the tip r_{t}.

With increasing loading, the evolution of plastic zone near the interfacial crack tip under loading mode (a) is shown in Fig. 3. Two dominant shear bands are activated from the crack tip and the crack surface, respectively, and they intersect inside the polymer. The rest of the material is either still in the elastic regime or has deformed plastically before and is now locked. Propagation of active shear bands with increasing load, as seen in Fig. 3 (b) and (c), takes place because of re-hardening of the material in the band and softening of the neighboring material.

The plastic zone is evidently different from that in the same but homogeneous polymer under mode I loading (Lai and Van der Giessen, 1997). While being symmetric with respect to the x_1-axis in the homogeneous medium, the plastic zone near the interfacial crack tip is offset and tilted away from the interface. In a homogeneous material, two shear bands are activated from the crack surface and intersect on the symmetry plane. With increased load, the plastic zone grows in an almost self-similar manner, with the origins of the two shear bands propagating along the crack surface in the negative x_1-direction. Simultaneously, the tip of the plastic zone moves forward along the symmetry plane.

The deviation of the plastic zone we find here for the interfacial crack is due to the constraint of the rigid substrate. The shear band originating from the crack surface propagates in the negative x_1-direction; but the other shear band is fixed at the crack tip. The shear band originating from the crack surface is more active than the other one as is clearly visible in Fig. 3(c), and its propagation is dominant as the loading is increased. This makes the plastic zone prone to develop away from the interface to relax the concentration of stress near the crack tip.

Fig. 4 shows the development of plastic zone under loading mode (b), in which only shear loading is applied. In the inital stage, a dominant shear band is activated at the crack tip and almost parallel to the interface. When the loading increases, shear bands are also activated from the crack surface, and multiple shear bands develop approximately parallel to the interface, as seen in Fig. 4(b) and 4(c). At the same levels of $|K|$, especially for the two higher values, the plastic zone under loading mode (b) is significantly larger than that under loading mode (a), thus providing more shielding of the crack tip as will be discussed later.

Under loading mode (c), shear loading is applied along the negative x_1-axis. In view of the blunted crack tip and the loading mode, it is not surprising to find that the initiation of the plastic zone is offset from the crack tip as shown in Fig. 5(a). Strain hardening inside the plastic zone compels the two main shear bands to expand along the crack surface, as shown in Fig. 5(b) and 5(c). In this case, the softening of material near the boundary of the plastic zone also activates shear bands perpendicular to the two dominant shear bands, as seen in Fig. 5(c). The expansion of the plastic zone from the crack surface to the crack tip and subsequent strain hardening there enhances the stress right in front of the crack tip.

4.2. Influence of softening and hardening

The softening–hardening characteristics also have some profound effects, as detailed for a mode I crack in a homogeneous polymer by Lai and Van der Giessen (1997). For an interfacial crack, their effects are quite similar, and only a brief consideration is therefore given for loading mode (a).

For an interfacial crack along material B, which shows continuous hardening after yield without softening, the plastic zone near the crack tip is shown in Fig. 6 at the same load level as in Fig. 3(b) for material A. Due to the absence of strain softening after yield, no shear band is activated near the crack tip. The strain hardening at the crack tip tends to depress both extent and intensity of the localization of plastic deformation, just like in a metal (cf., e.g., Shih, 1991; Tvergaard and Hutchinson, 1993). By contrast, in material C, which exhibits only softening after yield, multiple shear bands are activated from the crack tip and the crack surface as shown in Fig. 7. However, because of the absence of strain hardening, these shear bands do not propagate and the stress concentration near the crack tip is relaxed by localization in more and more shear bands.

The above results for materials A, B and C emphasize that softening and hardening are counteracting factors affecting the plastic deformation near an interfacial crack tip. Softening tends to intensify the localization of plastic deformation, while increasing strain hardening suppresses the local plastic shearing process and governs the propagation of shear bands. Loading mode and plastic-flow characteristics, including softening and hardening, together determine the position and the size of plastic zone, which affect the distribution of stress along interface.

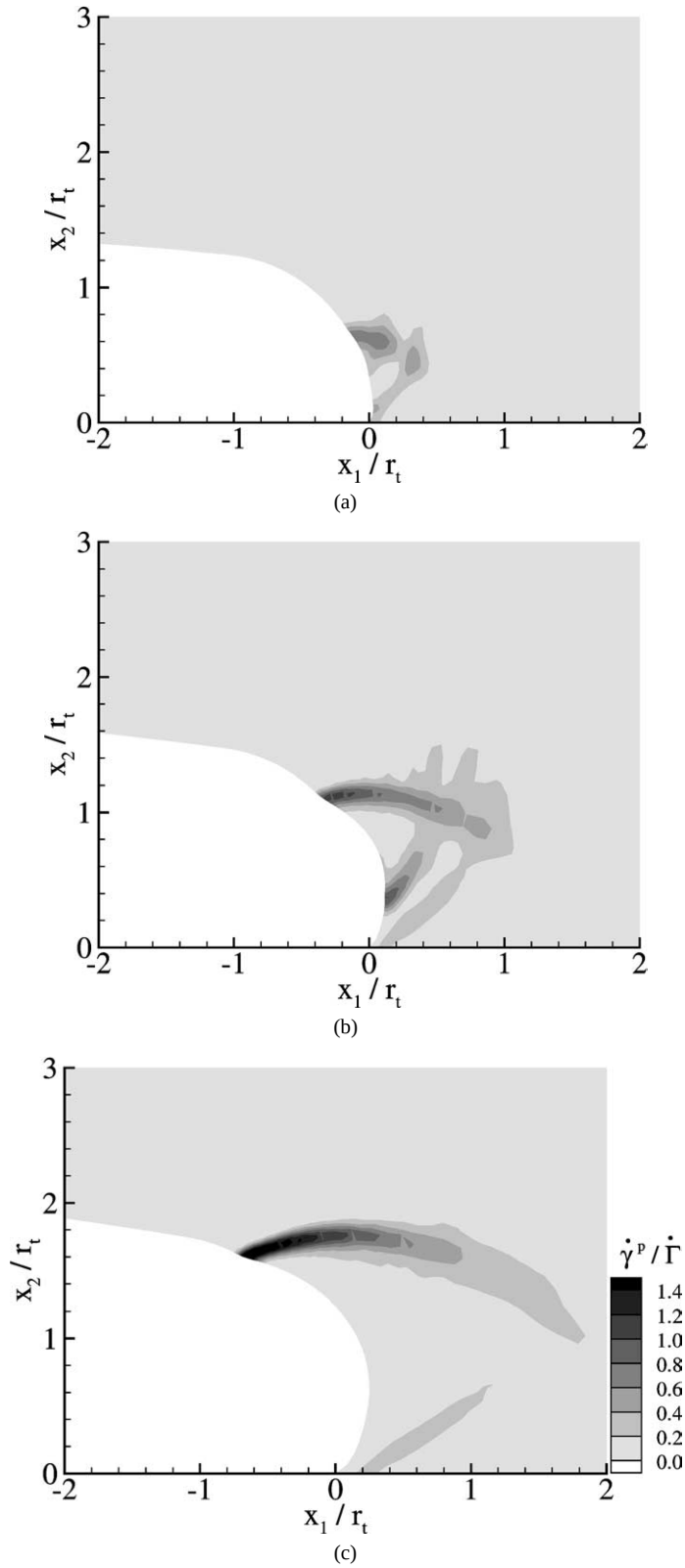

Fig. 3. Crack tip plastic zones under loading mode (a) in material A with (a) $|K|/K_0 = 1.5$, (b) 2.5, and (c) 3.5.

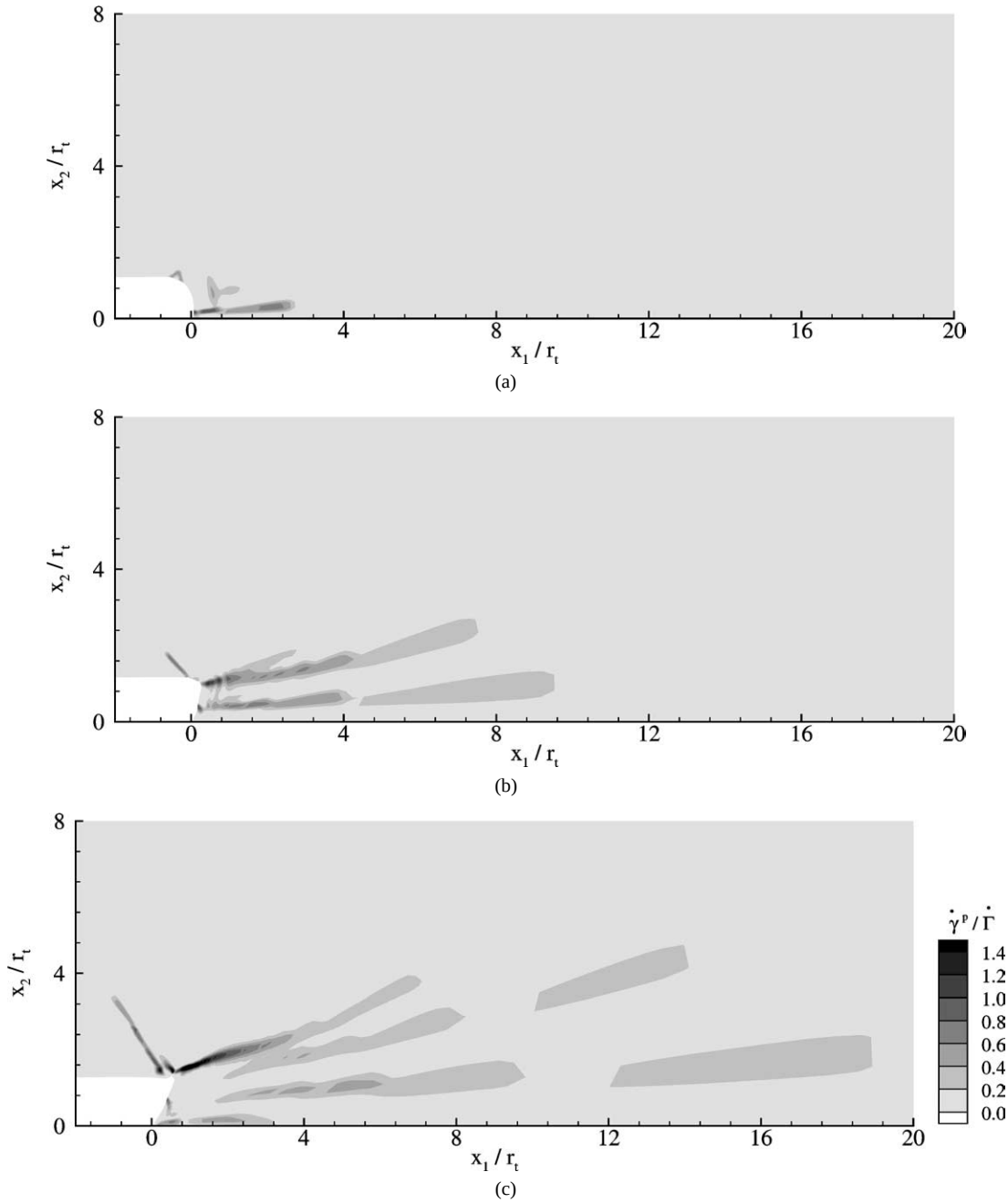

Fig. 4. Crack tip plastic zones under loading mode (b) in material A with (a) $|K|/K_0 = 1.5$, (b) 2.5, and (c) 3.5.

4.3. Normal stress distribution along interface

The distribution of the stress normal to the interface, σ_{22}, is critical to the delamination of the interface. In this section, we analyze the influence of plastic deformation on the interface normal stress.

Under loading mode (a), the distribution of normal stress along the interface, $x_2 = 0$, is given in Fig. 8. The load level shown, $|K|/K_0 = 2.5$, corresponds to Fig. 3(b) for material A and to Fig. 6 for material B; the elastic stress distribution is shown for comparison. It is found that plastic deformation near the crack tip relaxes the stress inside the plastic zone, and thus enhances the stress outside of the plastic zone compared with the elastic solution. The stress right near the inner surface of the notch in

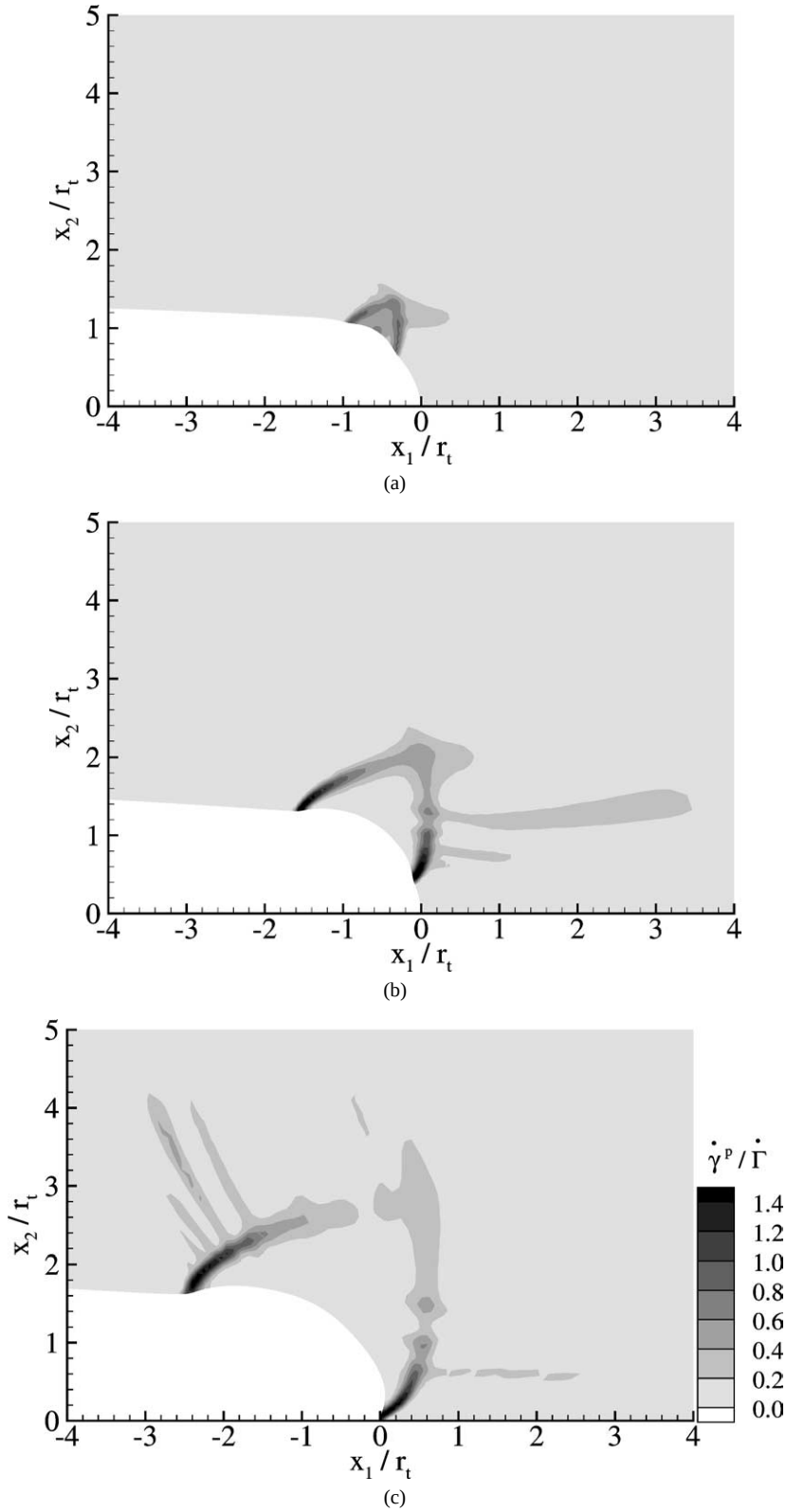

Fig. 5. Crack tip plastic zones under loading mode (c) in material A with (a) $|K|/K_0 = 1.5$, (b) 2.5, and (c) 3.5.

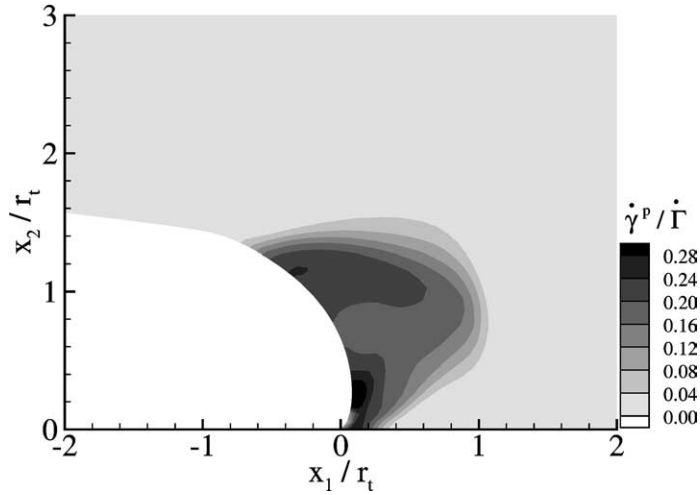

Fig. 6. Crack tip plastic zone in material B under loading mode (a) with $|K|/K_0 = 2.5$.

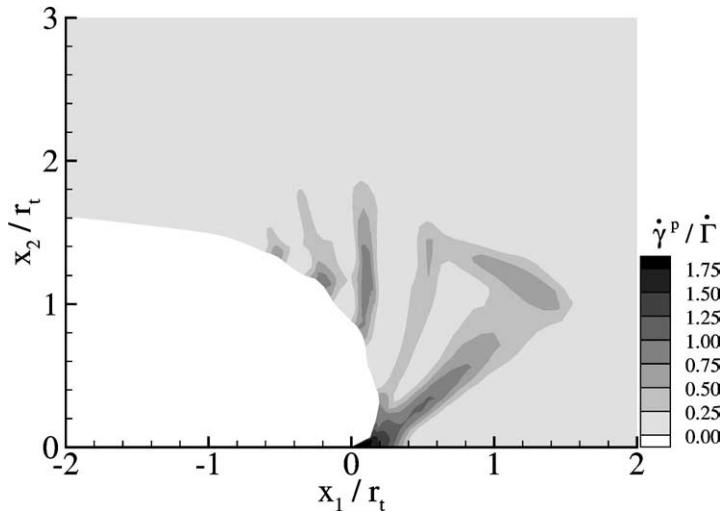

Fig. 7. Crack tip plastic zone in material C under loading mode (a) with $|K|/K_0 = 2.5$.

materials A and B is high at this load level since strain hardening has 'locked up' the material there. For this loading mode, the size of the plastic zone in material A (Fig. 3(b)) is comparable with that in material B (Fig. 6). However, because the material in softening state cannot sustain large stress, the softening effect enhances the stress in front of the crack tip compared with that in material B.

On the other hand, for the pure mode II loading, mode (b), with the same $|K|/K_0 = 2.5$, a larger plastic zone has developed along the interface in material A (Fig. 4) than in material B, which gives more stress relaxation right in front of the crack tip, as shown in Fig. 9.

However, for some negative mode mixities, plasticity can actually enhance the stress near the crack tip as shown in Fig. 10. For loading mode (c), the stress concentration zone for the elastic material is offset from the crack tip. But with increasing loading, the plastic zone evolves from the crack surface to the crack tip, Fig. 5, and causes hardening there, thus enhancing the near-tip stress compared with the elastic solution. From these examples, it can be seen that the development of the plastic zone near the interfacial crack tip strongly affects the distribution of normal stress along interface. For fracture mechanisms that are governed by the interface normal stress, the interplay between plastic dissipation and precipitation of crack growth are strongly dependent on mode mixity.

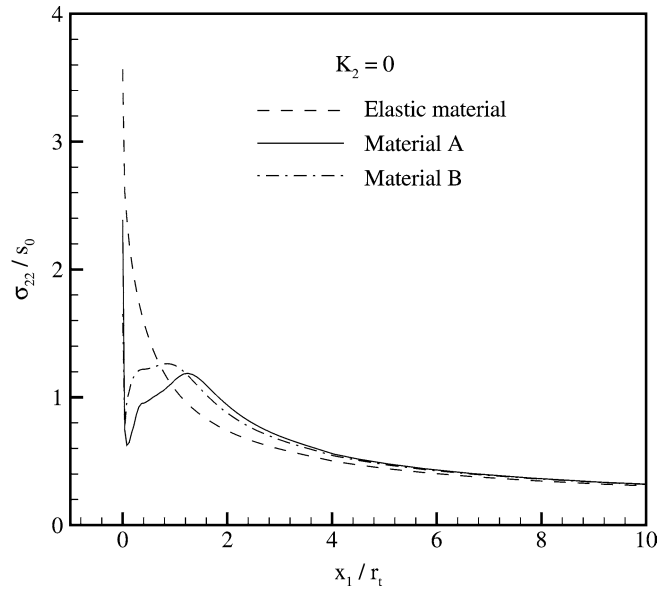

Fig. 8. Distribution of interface normal stress under loading mode (a) with $|K|/K_0 = 2.5$.

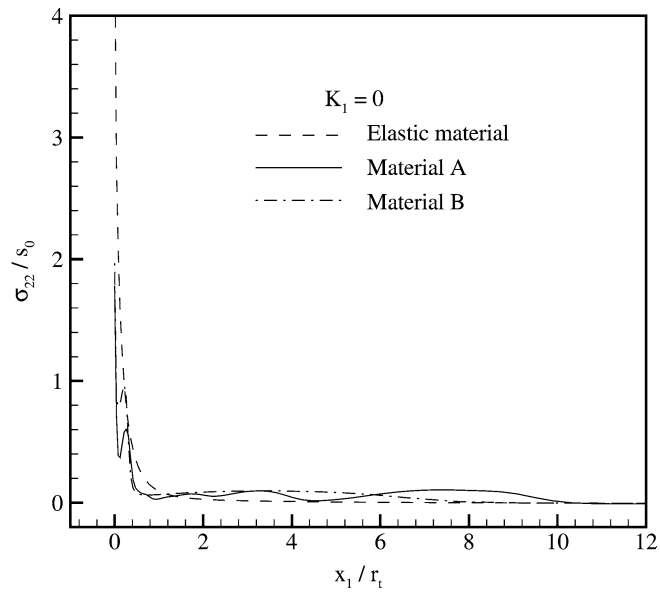

Fig. 9. Distribution of interface normal stress under loading mode (b) with $|K|/K_0 = 2.5$.

5. Interface toughness

Experiments have revealed that the toughness of a bi-material interface strongly depends on the mode mixity (Wang and Suo, 1990; Cao and Evans, 1989; Liechti and Chai, 1992). For the interface between a steel and an epoxy, the near mode II toughness has been found to be about 5 times higher than the near mode I toughness (Wang and Suo, 1990). It is well known that fracture toughness, in general, can inherit much from plastic dissipation in the material. Analyses of fracture of a ceramic–metal interface by Tvergaard and Hutchinson (1993) have revealed that plasticity enhances the interface toughness for all modes of loading, but substantially more so in the presence of a significant mode II component of loading than in near mode I condition.

Admitting that a thorough fracture analysis requires a cohesive model, such as adopted by Needleman (1990) and Tvergaard and Hutchinson (1993), we here choose a simpler post-processing type estimate based on the observation that fracture is

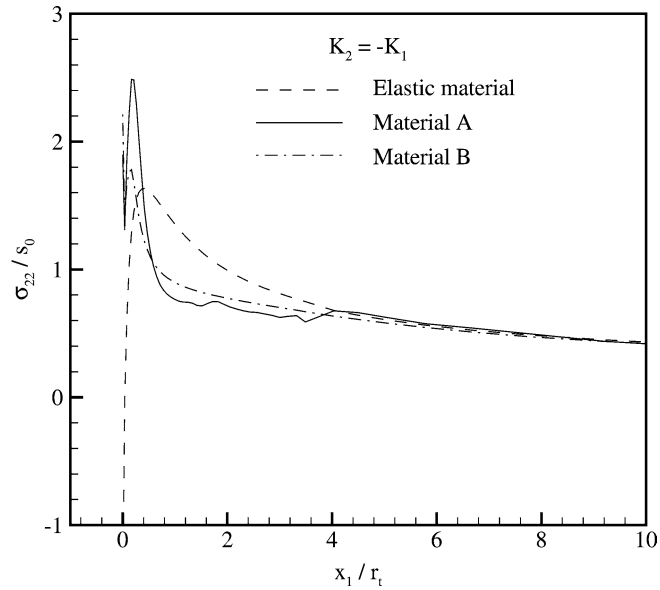

Fig. 10. Distribution of interface normal stress under loading mode (c) with $|K|/K_0 = 5.0$.

governed by the intrinsic work of separation and the cohesive strength. With $\sigma_{\rm cr}$ denoting the interface bond strength, the intrinsic toughness is governed by the product of $\sigma_{\rm cr}$ and a characteristic length scale $\delta_{\rm f}$. With these parameters, the critical stress intensity factor $K_{\rm cr}$ for which crack growth precipitates can be written in the following nondimensional form:

$$\frac{K_{\rm cr}}{K_0} = \mathfrak{F}\left(\frac{\sigma_{\rm cr}}{s_0}, \frac{\delta_{\rm f}}{r_{\rm t}}; \frac{s_0}{E}, \nu, \psi, \frac{s_{\rm ss}}{s_0}, \frac{As_0}{T}, \alpha, \frac{h}{s_0}, N, \frac{C^{\rm R}}{s_0}\right) \quad \text{with } K_0 = s_0\sqrt{r_{\rm t}}. \tag{24}$$

The simple implementation used here is that we take fracture to start when the normal stress on the interface, $\sigma_{22}(x_1, 0)$, attains the critical value $\sigma_{\rm cr}$ over a distance larger than $\delta_{\rm f}$. Once the critical stress intensity factor $K_{\rm cr}$ is determined, the interfacial fracture toughness $\mathcal{G}$ can be obtained from Eq. (18).

The values of the fracture properties $\sigma_{\rm cr}$ and $\delta_{\rm f}$ obviously depend on the material system and on the activated fracture mechanism. Here we focus on situations where cleavage of the polymer dominates, as was found in epoxy-glass systems by Swadener et al. (1999), where $\sigma_{\rm cr}$ is a few times larger than the athermal shear strength s_0 and the characteristic size of breaking fibrils is less than micrometers. We vary $\sigma_{\rm cr}/s_0$ between 1 and 3, and let $\delta_{\rm f}/r_{\rm t} = 0.01$ ($\delta_{\rm f} \approx 1$ μm for $r_{\rm t} = 0.1$ mm). As discussed by Swadener et al. (1999), the detailed physics of interfacial failure along polymer interfaces is quite complex and not very well mapped out (e.g., is the intrinsic fracture energy dependent on mixity?). Granted this situation, there is a good case for performing the simplifying analysis instead of using a cohesive zone model in order to get a qualitative feeling for the role of shear yielding on interfacial debonding.

For all loading cases considered here in material A and B, the fracture criterion formulated above is satisfied in the first element ahead of the crack tip, since the minimum element size is $\approx 0.04r_{\rm t}$. For the interface between material A and a rigid substrate, Fig. 11 shows the variation of critical stress intensity factor with mode mixity for different interface bond strengths $\sigma_{\rm cr}/s_0$. It is seen that the dependence of interface toughness on mode mixity is sensitive to the interface bond strength. For a relative poorly bonded interface, $\sigma_{\rm cr}/s_0 = 1$, the interface toughness varies slightly as the mode mixity increases from zero, while it increases strongly when the mode mixity is negative. With increasing interface bond strength, the toughness increases for all modes, but more significantly for near mode II ($\psi \to 90^\circ$) than for other modes. It seems that the interface bond strength governs the extent of plasticity that can develop near the interface. Only for a strongly bonded interface, can plasticity play a significant role.

To elucidate the contribution of plasticity to interface toughness more, the critical stress intensity factors for various materials on a rigid substrate are shown in Fig. 12. By comparing with the results included for an elastic material, we see that for this particular interface bond strength, $\sigma_{\rm cr}/s_0 = 2.7$, plasticity enhances the toughness for mode mixities larger than -20°, but has an embrittling effect for smaller ψ. Moreover, compared with material B, the softening effect before hardening in material A provides a larger contribution to the interface toughness for $\psi > 30^\circ$ or so, but a smaller contribution for other modes, which shifts the minimum interface toughness to near mode I. The noteworthy asymmetry of the mixity dependence of toughness

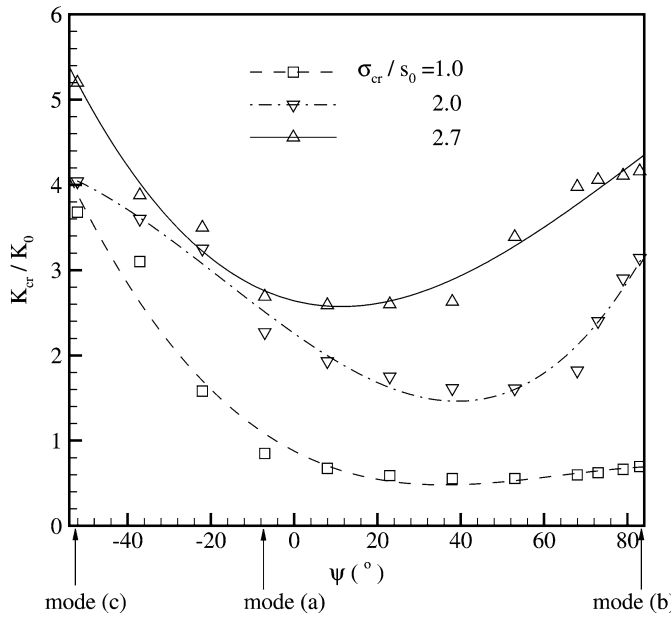

Fig. 11. Variation of critical stress intensity factor with respect to mode mixity for different bonding strengths.

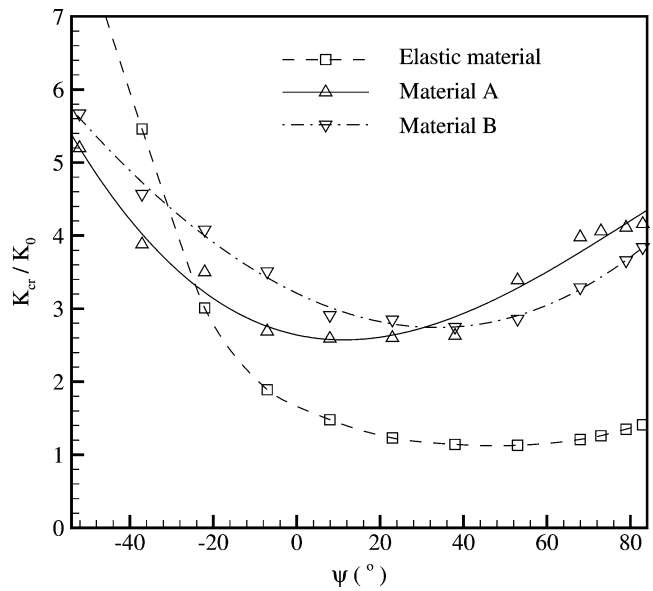

Fig. 12. Variation of critical stress intensity factor with respect to mode mixity for different interfaces.

revealed in Fig. 12 has also been found numerically and experimentally by Liechti and Chai (1992) and by Swadener et al. (1999).

These phenomena can be understood by the position and the size of plastic zone, and their influence on the interface normal stress as we have discussed in Section 4.3. For mode mixities larger than $-20°$, the stress concentration zone in the elastic material is located at the crack tip, and this is where yield initiates. Plastic deformation releases the intensity of stress near the crack tip as seen in Figs. 8 and 9, and a higher toughness is predicted compared with that of an elastic material. On the other hand, for mixities less than $-20°$, the elastic stress concentration zone is offset from the crack tip, and propagation of the plastic zone from crack surface to crack tip (cf. Fig. 5(c)) and subsequent hardening at this zone enhances the normal stress near the crack tip as shown in Fig. 10, thereby lowering the interface toughness. For a mode mixity larger than $30°$, the plastic zone along the interface in material A is much larger than that in material B, which gives more stress relaxation, see Fig. 9. For other

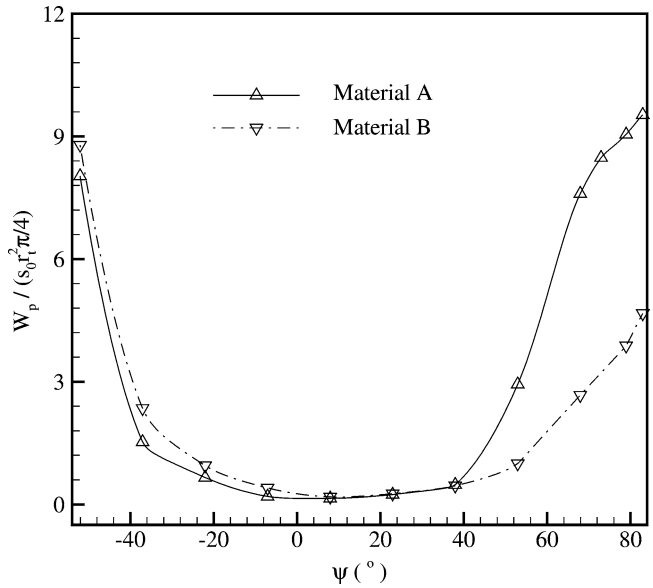

Fig. 13. Variation of dissipated plastic energy with respect to mode mixity at critical delamination.

modes, the softening effect in material A enhances the normal stress in front of the crack tip compared with that in material B as seen in Figs. 8 and 10.

The dissipated plastic energy W_p, calculated in the entire body using Eq. (12), until interface delamination is plotted as a function of mode mixity in Fig. 13. Comparison of Figs. 12 and 13 reveals that the dependence of the toughness of a perfectly bonded interface on mode mixity is quite well represented qualitatively by W_p (see also Swadener et al., 1999). This is true in particular for positive mode mixities, where most of the plastic deformation has developed to relax the near-tip stress.

6. Conclusion

In this paper, the mechanical behavior of glassy polymer is described by a constitutive model that accounts for its characteristic softening upon yield and the subsequent progressive hardening. The plastic deformation near a blunted crack tip between a glassy polymer and a rigid substrate is investigated, and the influence of plasticity on interface toughness is analyzed.

The numerical results show that the plastic zone near the interfacial crack tip is offset from the interface because of the constraint from the rigid substrate. The mode mixity affects the position of initial plastic yield and the direction of the subsequent development. The softening–hardening characteristics of plastic flow govern the way of the plastic zone propagation. Softening tends to intensify the localization of plastic deformation, while hardening tends to depress the local plastic deformation. These trends together with mode mixity control the normal stress along the interface.

When a simple fracture criterion, maximum interface normal stress over a critical distance,is adopted to determine the toughness, it is found that (i) the interface bond strength affects the sensitivity of toughness on mode mixity by controlling the extent of plasticity; and (ii) the contribution of plastic work to interface toughness depends on the mode mixity and the plasticity characteristics. For mode mixities larger than $-20°$, plasticity is found to enhance the interface toughness, but more significantly for higher mixities. However, for mode mixities less than $-20°$, plasticity has an embrittling effect. Compared with a material exhibiting hardening upon yield without softening (i.e., like a metal), the softening effect in polymer increases the toughness of higher mode mixities, while it tends to make the material more brittle for other modes.

Compared with the experiment results on steel/epoxy interface toughness (Wang and Suo, 1990), in which only data for mode mixities larger than $-20°$ is available, the present numerical simulations predict a quite similar dependence of interface toughness on mode mixity, but somewhat smaller in value. However, it was also noticed that in this experiment the toughness rises more slowly with mode mixity when the metal becomes harder. Therefore, for the interface between a polymer and a rigid substrate in our work, the smaller increase of interface toughness with mode mixity than seen experimentally is reasonable. These findings are further consolidated by comparing with the experimental results by (1999) on epoxy-glass interfaces. Our results are consistent with the asymmetric mode-mix dependence of toughness found experimentally, but the toughening effect is

again smaller than seen experimentally. It should be noted, however, that no effort has been made to fit the plasticity parameters to the materials used in the experiments.

Acknowledgements

This research was supported by the Technology Foundation STW, applied science division of NWO and the technology programme of the Ministry of Economic Affairs in the Netherlands.

References

Argon, A.S., 1973. A theory for the low-temperature plastic deformation of glassy polymers. Philos. Mag. 28, 839–865.
Arruda, E.M., Boyce, M.C., 1993. A three-dimensional constitutive model for large stretch behavior of rubber materials. J. Mech. Phys. Solids 41, 389–412.
Basu, S., Van der Giessen, E., 2002. A thermo-mechanical study of mode I, small-scale yielding crack-tip fields in glassy polymers. Int. J. Plasticity 18, 1395–1423.
Bowden, P.B., 1973. The yield behavior of glassy polymers. In: Haward, R.N. (Ed.), The Physics of Glassy Polymers. Applied Sciences, Essex, pp. 279–295.
Boyce, M.C., Parks, D.M., Argon, A.S., 1988. Large inelastic deformation of glassy polymers, Part I: rate dependent constitutive model. Mech. Mater. 7, 15–33.
Cao, H.C., Evans, A.G., 1989. An experimental study of the fracture resistance of bimaterial interfaces. Mech. Mater. 7, 295–304.
Hutchinson, J.W., Evans, A.G., 2000. Mechanics of materials: top-down approaches to fracture. Acta Mater. 48, 125–135.
Lai, J., Van der Giessen, E., 1997. A numerical study of crack-tip plasticity in glassy polymers. Mech. Mater. 25, 183–197.
Liechti, K.M., Chai, Y.S., 1992. Asymmetric shielding in interfacial fracture under in-plane shear. J. Appl. Mech. 59, 295–304.
Needleman, A., 1990. An analysis of tensile decohesion along interface. J. Appl. Mech. 38 (3), 289–324.
Rice, J.R., 1988. Elastic fracture mechanics concepts for interfacial cracks. J Appl. Mech. 55, 98–103.
Shih, C.F., 1991. Crack on bimaterial interfaces: elasticity and plasticity aspects. Mater. Sci. Engrg. A 143, 77–90.
Swadener, J.G., Liechti, K.M., De Lozanne, A.L., 1999. The intrinsic toughness and adhesion mechanisms of a glass-epoxy interface. J. Mech. Phys. Solids 36, 112–147.
Tvergaard, V., Hutchinson, J.W., 1993. The influence of plasticity on mixed mode interface toughness. J. Mech. Phys. Solids 41, 1119–1135.
Wang, J.S., Suo, Z., 1990. Experimental determination of interfacial toughness curves using brazil-nut-sandwiches. Metall. Mater. 38, 1279–1290.
Wei, Y., Hutchinson, J.W., 1999. Models of interface separation accompanied by plastic dissipation at multiple scales. Int. J. Fract. 95, 1–17.
Wu, P.D., Van der Giessen, E., 1993. On improved network models for rubber elasticity and their application to orientation hardening in glassy polymers. J. Mech. Phys. Solids 41, 427–456.
Wu, P.D., Van der Giessen, E., 1996. Computational aspects of localized deformations in amorphous glassy polymers. Eur. J. Mech. A 15, 799–823.